Available online at www.sciencedirect.com
SCIENCE DIRECT
ELSEVIER
Earth and Planetary Science Letters 240 (2005) 732–747
EPSL
www.elsevier.com/locate/epsl

Palaeomagnetic data from Ediacaran (Vendian) sediments of the Arkhangelsk region, NW Russia: An alternative apparent polar wander path of Baltica for the Late Proterozoic–Early Palaeozoic

María Paula Iglesia Llanos [a,*], Jennifer Alice Tait [a], Viktor Popov [b], Alexandra Abalmassova [a]

[a] *Department for Earth and Environmental Sciences, Geophysics Section, Ludwig-Maximilians-Universität München, Theresienstrasse 41, 80333 Munich, Germany*
[b] *Department for Palaeomagnetic Reconstructions, All-Russia Petroleum Research Exploration Institute (VNIGRI), Liteiny Ave., 39, St. Petersburg, 191104, Russia*

Received 24 August 2004; received in revised form 25 July 2005; accepted 1 September 2005
Available online 11 November 2005
Editor: E. Boyle

Abstract

The study area is situated along the Zolotica river in NW Russia, located within the Kola–Dvyna Rift System in the Baltic Shield that developed during Meso and Neoproterozoic times. A 9-m thick section made up of shallow marine sediments of Upper Ediacaran age was sampled in this locality. Two volcaniclastic levels from the middle part of the section yielded an age of ~556 Ma. (U/Pb SHRIMP-II on zircons). Two magnetic components were successfully isolated, component A (Decl=157.1, Incl=68.0, α_{95}=1.9°, N=575 in situ) carried by magnetite and component B (Decl=120.3, Incl=−31.7, α_{95}=3.9°, N=57, bedding corrected), carried by haematite. While component A is thought to represent a younger overprint direction, the in situ direction for component B on the other hand, is dissimilar to any expected younger direction and is considered to be primary magnetisation in origin, acquired during or soon after deposition of the sediments in the Late Ediacaran. The corresponding palaeomagnetic pole for component A in situ is located at Lon=55.4°E, Lat=31°N, A_{95}=2.7° and for component B at Lon=110°E, Lat=28.3°S, A_{95}=3.8°, N=57. Combined with other palaeomagnetic poles of the same tectonostratigraphic unit an alternative apparent polar wander path for the Late Proterozoic–Early Palaeozoic of Baltica is proposed. Such an alternative path shows that after the mid Cryogenian (750 Ma), the poles that were situated over South Africa (p.d.c.) moved to the east until they reached Australia during the Late Ediacaran (555 Ma) where they remained approximately stationary until the beginning of the Cambrian (~545 Ma). Finally, they moved to the northwest until they reached the Arabian Peninsula in the Early Ordovician. Palaeolatitudes indicate that Baltica situated near the equator from the Cryogenian through to the Ediacaran moving gradually to the south at c. 1 cm/yr. During the Late Early Ediacaran, the plate suddenly began to drift northward at c. 8 cm/yr and in the boundary with the Cambrian it was positioned in low to intermediate latitudes. Finally, Baltica began to move back to the south at c. 13 cm/yr until in the Early Ordovician, reaching intermediate to high southern latitudes.

Keywords: Ediacaran; Baltica; palaeomagnetism; Neoproterozoic

* Corresponding author. Ingeodav, Depto. Ciencias Geológicas, Fac. Ciencias Exactas y Naturales, UBA, Pab.2, Ciudad Universitaria, C1428EHA, Buenos Aires, Argentina. Fax: +54 11 4788 3439.
E-mail address: mpiglesia@gl.fcen.uba.ar (M.P.I. Llanos).

0012-821X/$ - see front matter © 2005 Elsevier B.V. All rights reserved.
doi:10.1016/j.epsl.2005.09.063

1. Introduction

There are still many questions regarding the reliability of the apparent polar wander (APW) path of Baltica for the Late Proterozoic–Early Palaeozoic due to the lack of reliable and well dated palaeomagnetic poles. The most widely used database for Baltica is that given by Torsvik et al. [1] and places Baltica at very high latitudes in the southern hemisphere throughout this time period, except for a short interval in the Late Ediacaran (560–550 Ma). The main problem with this dataset, however, is that it contains very few high quality data for the Ediacaran and Cambrian Periods, thus this section of the path relies on interpolations and palaeopoles whose reliability have been questioned in the literature.

On the basis of more recently published data, however, an alternative APW path for Baltica has been proposed by Popov et al. [2], which is in marked contrast to the APW path suggested by Torsvik et al. [1]. According to this model, Baltica was positioned at very low to intermediate latitudes during the Late Proterozoic to Early Palaeozoic.

The key to this problem concerning the palaeomagnetic dataset for Baltica is to obtain new data from well-dated sequences.

In this study, a sedimentary section exposed along the Zolotica river which is located to the NE of Arkhangelsk, NW Russia, was sampled. From these sediments, it was possible to obtain a radiometric age (U/Pb on zircons) of ~556 Ma as well as palaeomagnetic data which are of very good quality and similar to data obtained from Late Ediacaran rocks [2] exposed along the Winter Coast (555 ±3 Ma) situated some 70 km to the west (Fig. 1) of the Zolotica section, and also to recently published Ediacaran data from Ukraine [3].

2. Geological setting and palaeomagnetic sampling

The sampling area (65°36′N; 40°29′E) is located in the Kola–Dvyna Rifts System (Fig. 1) in the pericratonic area of the Russian Platform, that extends from the area of Arkhangelsk in the south to the Barents Sea in the north. The basement, made up of metamorphic rocks of Archean–Lower Proterozoic age, crops out in the westernmost area of Arkhangelsk. During the Late Proterozoic, northwestern-oriented rifts developed which produced the characteristic horst-and-graben structural style of the regional basement bounded by transform faults (Fig. 1). Sedimentation began in the area approximately at 750 Ma with sandstones and siltstones. In the Ediacaran, higher regional subsidence rates resulted in

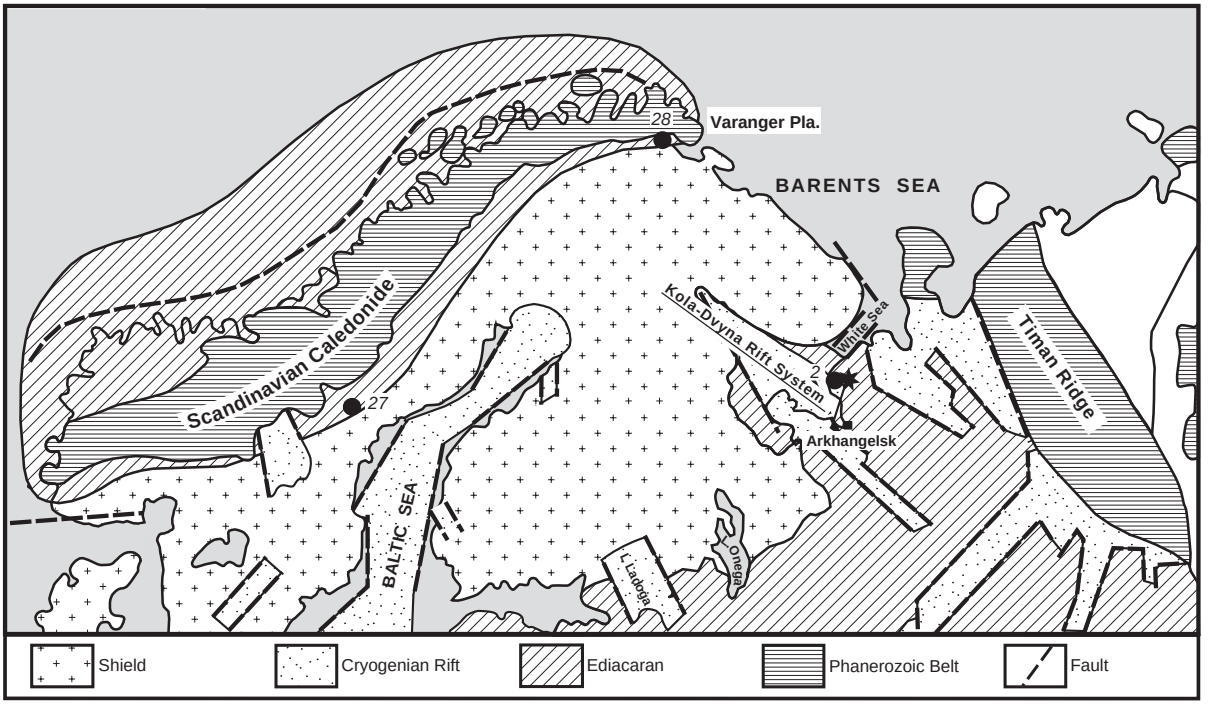

Fig. 1. Geological sketch map of Baltica and location of the study area (star), located within the Ediacaran Kola–Dvina Rift System which developed in the Late Proterozoic. Modified from Vidal and Moczydlowska [37]. Solid circles = other Ediacaran localities mentioned in the text and corresponding reference.

deposition of most of the sedimentary cover which reached thicknesses of up to 1200 m of terrigenous to shallow marine facies. The Ediacaran succession is overlaid partly by terrigenous and carbonate sediments of Devonian to Permian age and partly by glacial and marine Quaternary sediments.

During the Late Devonian, an important compressional tectonic event took place producing the uplift of the Kola–Dvyna block with associated magmatism. Such magmatism in fractures was mainly alkaline–ultramafic and was responsible for the formation of the diamond-bearing kimberlites from the diamondiferous province of Arkhangelsk [4,5].

The succession that crops out along the Zolotica river is several hundred meters thick. It increases in grain and strata thickness up-section, and lithologies

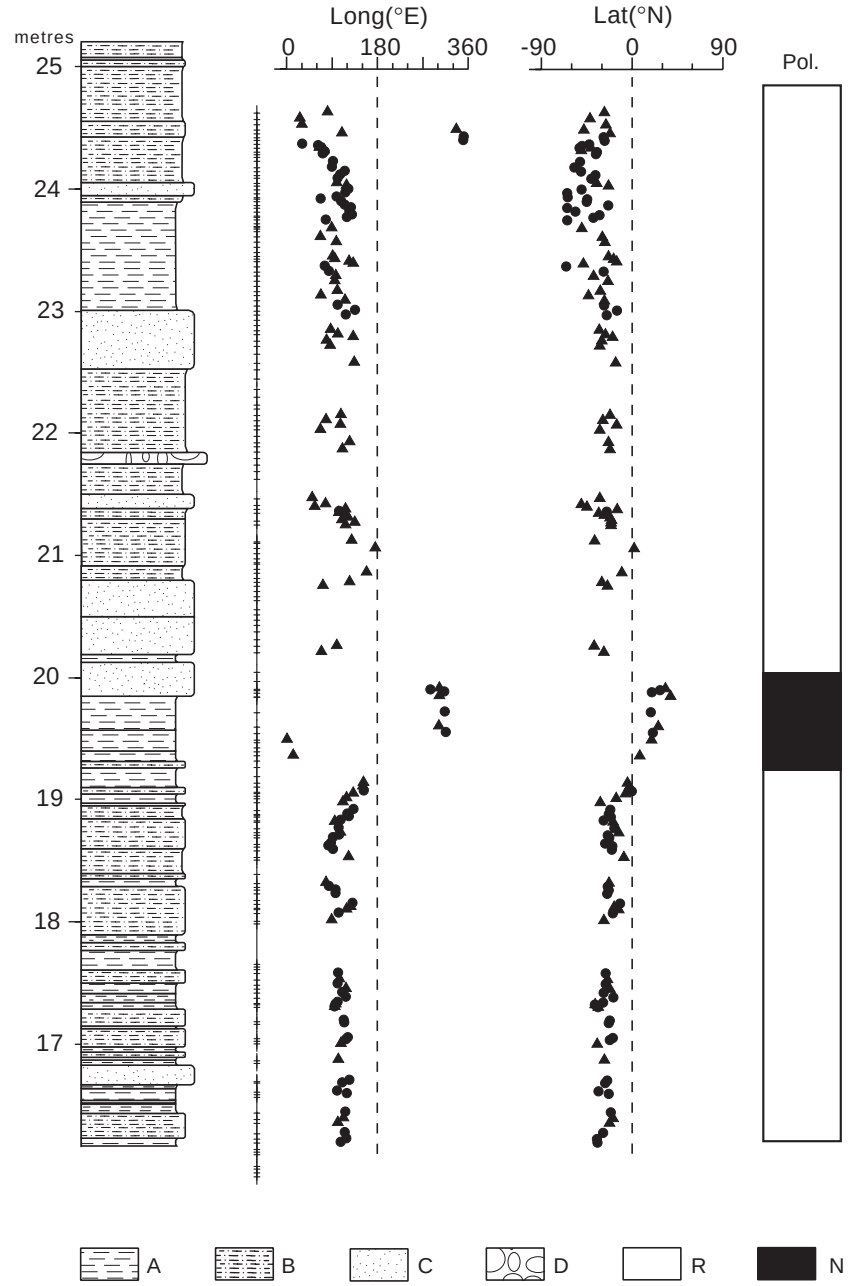

Fig. 2. Stratigraphical column of the Zolotica section (left). To the right, sampling sites (dash), Longitude/Latitude of VGPs and recorded polarities. A = claystone, B = clay-sandstone, C = sandstone, D = conglomerate, N = normal polarity; R = reverse polarity. Circles (triangles) in Long/Lat = sites with number of samples ≥3 (≤2).

consist of red and gray–green coloured sediments: laminated claystones and siltstones (open shallow marine facies), non-lithified sandstones in forestepping clinoforms (prodelta facies) and horizontal bedded sandstones (sandy shoal). It is practically unaffected by tectonic deformation and exhibits a north–south strike dipping up to 9° to the west.

For the present study, a c. 9-m thick section was sampled almost continuously (Fig. 2). In total, 190 levels were sampled with a distance ≤1 cm in the fine-grained sandstones and siltstones and ≤5 cm in the coarse-grained sandstones. As lithologies are rather fragile and drilling was not possible, hand samples were collected from which at least three 2 × 2 × 2 cm cubes were subsampled per sampling level.

3. Petrography

Microscopic analysis reveal that the sampled sediments are mainly claystones and sandstones with volcanic input. They are composed of some lithic fragments, as well as crystals of which quartz, feldspar, pyroxene and amphibole are the most common, with zircon, apatite, garnet, epidote and magnetite as accessory minerals. The size range of the crystals is typically 50–100 μm. The idiomorphic shape of some minerals such as zircons and apatite suggests the vicinity of a volcanic source area at the time of deposition.

The cement is composed in the red sediments, of haematite, and in the green-gray, of carbonate. To a lesser degree, in very fine-grained rocks the groundmass is made up of highly altered volcanic glass. Haematite and magnetite form the ferromagnetic fraction. The first appears as aggregates as well as a patina coating the other minerals, whereas the magnetite crystals show idiomorphic habitus.

4. Geochronology

Fresh idiomorphic zircons of primary magmatic origin were separated from two samples, ZL105 (21.2 m from the base) and ZL129 (22.5 m), respectively, for dating purposes.

Zircon crystals were hand selected and mounted in epoxy resin together with chips of the TEMORA (Middledale Gabbroic Diorite, New South Wales, Australia) and 91500 (Geostandart zircon) reference zircons. The grains were sectioned approximately in half and polished. Reflected and transmitted light photomicrographs and cathodoluminescence (CL) SEM images were prepared for all zircons. The latter were used to analyse the internal structures of the sectioned grains and to target specific areas within these zircons (Fig. 3).

U/Pb analyses were performed using SHRIMP-II ionmicroprobe (Center of Isotopic Research, VSEGEI, St. Petersburg, Russia). Each analysis consisted of five scans through the mass range, diameter of spot was about 18 km, primary beam intensity was about 4 nA. The data have been reduced as described by Williams ([6] and references therein), using the SQUID Excel Macro [7]. The Pb/U ratios have been normalized relative to a value of 0.0668 for the $^{206}Pb/^{238}U$ ratio of the TEMORA reference zircons, equivalent to an age of 416.75 Ma [8]. Uncertainties calculated for the concordia ages are reported at 2-σ level. The Wetherill [9] concordia plot (Fig. 4) has been prepared using ISOPLOT/EX [10].

The separated crystals range from rounded grains showing high degrees of corrosion and which are clearly detrital in origin, to very clear elongate prismatic

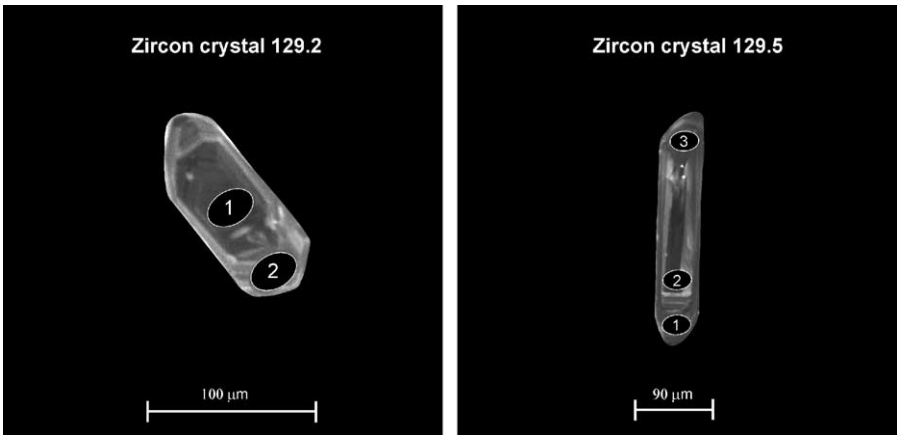

Fig. 3. Cathodoluminiscence SEM image of zircon crystals 129.2 and 129.5 (Center of Isotopic Research, VSEGEI, St. Petersburg, Russia) showing good prismatic habitus, from which a reliable age of the sediments at Zolotica has been determined.

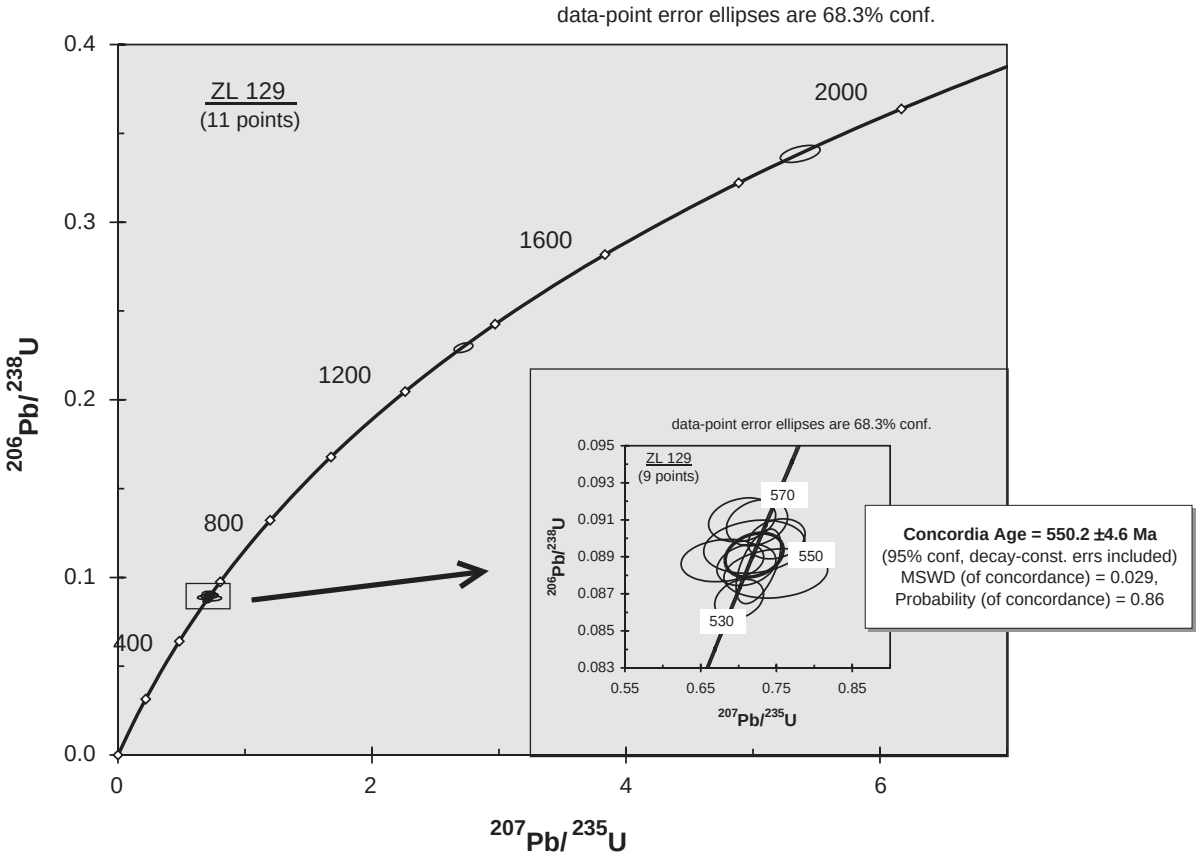

Fig. 4. Wetherill's [9] concordia plots of U/Pb SHRIMP-II analytical data from samples ZL129 (22.5 m from the base). Ellipses represent 1-sigma uncertainties for individual spots (measured points) but thick-line ellipse (concordia age) represents 95% confidence limit for ZL129.

crystals with good crystal habitus (Fig. 3). Few of the grains selected show any internal structure under reflected light; cathodoluminescence imaging, however, reveals the often complex internal structures. A total of 11 crystals were selected for analysis, four of which correspond to the clearly detrital grains. Analyses of these grains (105.2, 105.3, 129.1 and 129.3; Table 1) record ages ranging from 1.33 to 1.93 Ga, i.e. Palaeo- to Mesoproterozoic in age. The two older ages obtained are fairly typical for the Svecofennian domain and are to be expected for younger sediments of the Baltic shield. The two younger ages of 1.46 Ga and 1.33 are slightly more difficult to correlate with an event in Baltica. However, ages of 1.4 Ga have previously been reported from the Kola Peninsula, and SW Scandinavia [11–13], and the age distribution is similar to that obtained in previous studies from sedimentary sequences in southern Baltica, although these are somewhat distal to the current study area. In a recent statistical analysis of available detrital zircon data, the results obtained here fall within the distribution of ages which may be expected from Baltica, albeit at the upper and lower limits of the probability density curves [14]. However, given the possibility of Pb loss in the samples analysed, some of which are cracked and corroded, there may be inherent errors, thus further discussion and speculation of these Mesoproterozoic ages is not considered warranted.

The other 7 crystals selected are predominantly elongate and show varying degrees of corrosion. Grain 105.4 shows fairly good crystal habitus and magmatic zoning but the shot point is rather close to a crack in the crystal which can result in lead loss. The most prismatic crystal with the best crystal habitus and showing good magmatic zoning in both reflected light and CL imaging, is crystal 129.5 (Fig. 3). Three points were shot in this grain, unfortunately two over cracks which may result in lead loss, but shot 129.5.1 is solely within the magmatic zoning and is considered one of the most reliable ages obtained. Grain 129.2 also shows good crystal habitus and magmatic zoning in both reflected and CL imaging, and it contains a few inclusions. Two points were measured in the centre and the rim of this grain. The remaining four grains are all fairly

Table 1
U/Pb SHRIMP-II dataset from zircon crystals ZL 129 and ZL 105

Grain spot	$\%^{206}Pb_c$	U (ppm)	Th (ppm)	$^{232}Th/^{238}U$	(1) $^{206}Pb/^{238}U$ age	(2) $^{206}Pb/^{238}U$ age	(3) $^{206}Pb/^{238}U$ age	% Disc.	(1) $^{206}Pb^*/^{238}U$	±%	Err corr
zl129.1.1	0.21	240	65	0.28	1331.1 ± 9.4	1331.0 ± 10	1331.4 ± 9.7	1	0.2293	0.78	.427
zl129.2.1	1.02	190	138	0.75	552.9 ± 5.6	553.0 ± 5.4	555.3 ± 6.1	−2	0.08955	1.1	.173
zl129.2.2	0.46	366	257	0.73	555.3 ± 4.2	554.2 ± 4.2	556.8 ± 4.7	10	0.08997	0.79	.240
zl129.3.1	0.39	140	88	0.65	1879.0 ± 15	1879.0 ± 17	1880.0 ± 16	0	0.3385	0.94	.481
zl129.4.1	0.41	370	259	0.72	546.6 ± 7.9	545.9 ± 8.0	548.2 ± 8.9	7	0.0885	1.5	.560
zl129.4.2	0.82	350	244	0.72	536.1 ± 4.2	535.8 ± 4.2	539.2 ± 4.7	3	0.08671	0.82	.268
zl129.5.1	0.61	363	135	0.38	560.5 ± 4.9	561.2 ± 4.9	562.4 ± 5.1	−7	0.09084	0.91	.246
zl129.5.2	0.75	339	156	0.47	547.0 ± 4.4	547.2 ± 4.3	548.1 ± 4.6	−2	0.08856	0.83	.230
zl129.5.3	0.89	354	221	0.65	548.4 ± 4.5	550.4 ± 4.3	551.9 ± 4.7	−28	0.08880	0.85	.161
zl129.6.1	0.77	318	119	0.39	561.4 ± 4.6	563.2 ± 4.6	563.8 ± 4.8	−22	0.09100	0.86	.208
zl129.7.1	0.68	267	118	0.46	544.3 ± 5.2	542.2 ± 4.9	545.0 ± 5.2	18	0.08810	1.0	.165
zl105.2.1	0.67	180	131	0.75	1465.0 ± 12	1458 ± 12	1475.0 ± 13	5	0.2551	0.89	.448
zl105.3.1	0.65	130	109	0.87	1934.0 ± 17	1936 ± 20	1983.0 ± 20	0	0.3499	1.0	.502

Errors are 1-sigma; Pb_c and Pb* indicate the common and radiogenic portions, respectively. Error in standard calibration = 0.35%.
(1) Common Pb corrected using measured ^{204} Pb.
(2) Common Pb corrected by assuming ^{206} Pb/^{238} U–^{207} Pb/^{235} U age-concordance.
(3) Common Pb corrected by assuming ^{206} Pb/^{238} U–^{208} Pb/^{232} Th age-concordance.

elongate, but are fairly corroded and of detritic appearance and in general do not have good internal structures, and grain 129.6 appears to have an inherited core. On comparison with the results obtained, it can be seen that the points associated with crystal fractures do yield slightly younger ages. As it is not possible to test for lead loss in these samples given their relatively young age, these points are discounted due to the uncertainty. Also omitted from consideration are those grains which may have inherited cores, and those which have poor internal structures and are of corroded appearance. While grain 129.2 contains some inclusions, the results from both points yield almost identical ages (Table 1); these data, therefore, are considered reliable. Thus, the shot points considered the most reliable are 129.5.1, 129.2.1 and 129.2.2 (Table 1, Fig. 3). Combining these data results in a weighted mean of ~556 Ma. As these results are obtained from crystals which show only limited amounts of corrosion, this is considered to be close to the rock age.

5. Laboratory procedures

For the palaeomagnetic study, a total of 640 specimens were processed and analysed in the Munich University palaeomagnetic laboratory. Palaeomagnetic measurements were carried out using a 2G-Cryo magnetometer and for the corresponding analysis, the software developed in the Munich and Utrecht laboratories. In addition, rock magnetic studies were performed using a variable frequency translation balance (VFTB) and a KLY-2 Kappabridge magnetic susceptibility meter (15 positions).

5.1. Rock magnetic studies

Specimens of red and green-gray-coloured sediments were processed with the VFTB in order to get hysteresis (maximum field = 300 mT) and thermomagnetic curves. In Fig. 5, representative examples of red and green-gray sediments show their distinct rock magnetic properties. In the case of the red sediments, hysteresis loops reveal that the magnetic contribution is provided by at least two minerals, with high and lower coercivity, respectively, showing either pot-belly (Fig. 5a) or wasp-waist geometry that are not saturated at 300 mT. The corresponding thermomagnetic curves show the high coercivity mineral is dominant and has Curie temperature (T_c) ≈ 650 °C (haematite). Green-gray sediments on the other hand, display hysteresis loops which show the contribution of mainly the paramagnetic minerals and secondly, of a ferromagnetic mineral (Fig. 5b). The latter is interpreted to be magnetite, according to the H_c (~10 mT) and the corresponding thermomagnetic curves (T_c ≈ 580 °C).

5.2. Palaeomagnetic studies

Specimens have been treated using either conventional stepwise thermal techniques (Fig. 6) or alternating field (AF) demagnetisation. However, AF treatment was generally not very successful in revealing the full spectrum of the magnetisations, thus most samples were subjected to thermal demagnetisation.

The data presented in this paper and discussed hereinafter derive from fine to medium-grained red sediments as the coarse-grained and green-gray coloured

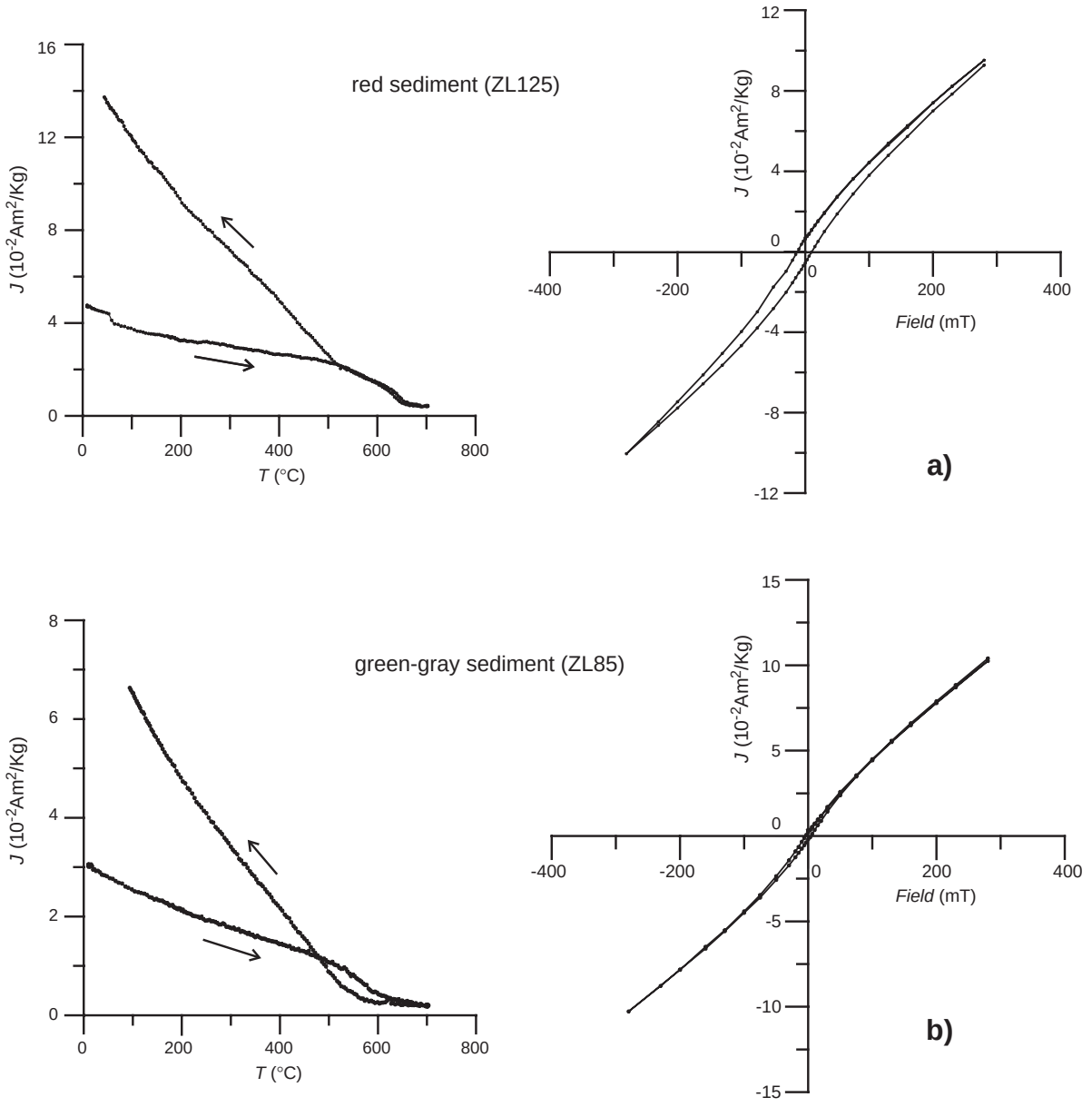

Fig. 5. Red and green-gray sediments show distinct rock magnetic properties. Red sediments show at least two minerals, with high and lower coercivities, respectively, that produce either (a) pot belly or wasp-waisted hysteresis loops which are not saturated at 300 mT. The corresponding thermomagnetic curve shows that the dominant high coercivity mineral has Curie temperature (T_c) ≈ 650 °C, typical of haematite. Green-gray sediments on the other hand, reveal (b) that the contribution belongs mostly to the paramagnetic minerals plus a ferrimagnetic mineral which is interpreted as magnetite, based on the H_c (~10 mT) and corresponding thermomagnetic curves (T_c ≈ 580 °C).

sediments do not yield reliable results. Such a difference in the palaeomagnetic behaviour between red and green-gray sediments resides in the fact that the dominant magnetic carriers are different for each case, i.e., haematite in the red and magnetite in the green-gray sediments (Fig. 5).

Samples were heated up to maximum temperatures of 710 °C; after c. 650 °C temperature steps of 3 °C were used (Fig. 6). The palaeomagnetic analysis has been performed using principal component analysis [15]. Two magnetic components (Figs. 6 and 7) were consistently isolated: (i) component A showing (Fig. 7a) mostly a southerly direction with positive inclinations (Decl=157.1, Incl=68.0, α_{95}=1.9°, N=575 in situ and Decl=171.4, Incl=66.9 after bedding correction), which was removed by 580 °C (magnetite) and

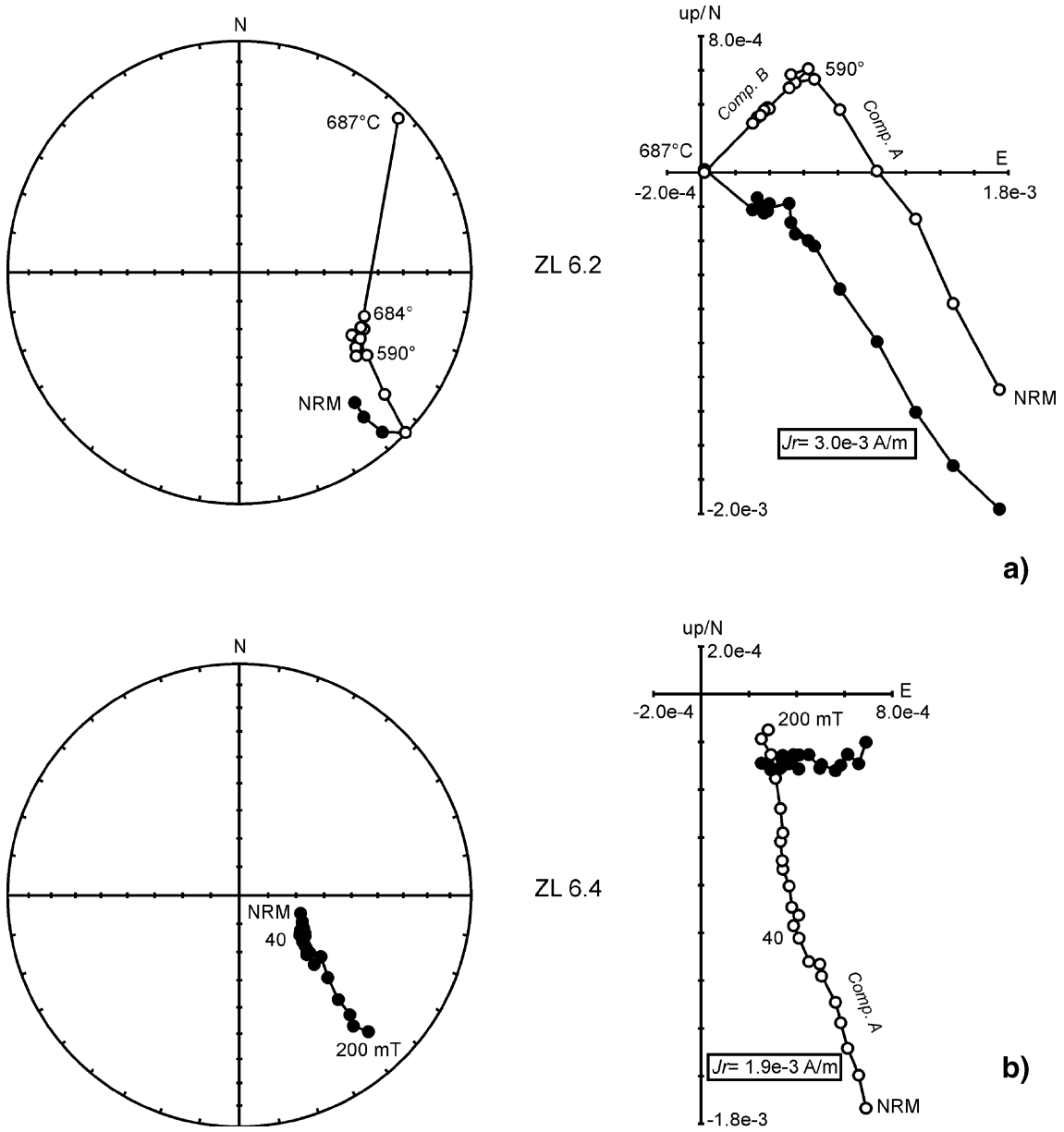

Fig. 6. Specimens show two clear magnetic components. Component A has mainly southerly declinations with positive inclinations carried by magnetite (unblocking temperatures ~580 °C), and component B shows mainly south-eastern declinations with negative inclinations as well as opposite directions, carried by haematite (unblocking temperatures ≥650 °C). Open (solid) circle = upper (lower) hemisphere. J_r = NRM intensity in Amperes/meter.

(ii) component B (Fig. 7b) identified with dual polarities, yielding south easterly (north westerly) declinations and intermediate negative (positive) inclinations and erased between 630 and 690 °C (haematite). The in situ A direction coincides with that expected for the Lower Ordovician in the region and therefore component A is considered to be an overprint of possible Early Ordovician. The origin of an Ordovician remagnetisation is very difficult to explain geologically and there is no apparent evidence for any alteration in the rocks studied which could relate to a remagnetisation event of any age. The possibility of an Ordovician age for this overprint therefore, is based purely upon the fact that its palaeopole coincides with the well established Ordovician pole for Baltica.

The reversal test [16] was applied to component B from sites which reveal only fully normal or inverse mean directions in the intervals 16.3–17.7 m, 19.6–20.0

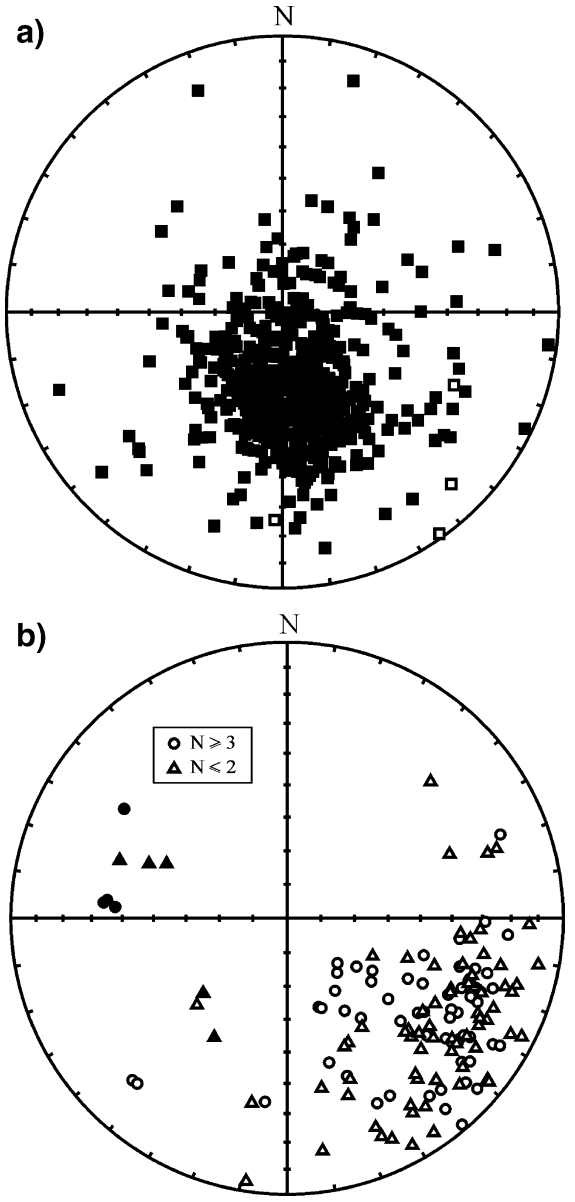

Fig. 7. Stereoplots showing (a) in situ directions from component A (N=575) and (b) bedding corrected mean site directions (msd) from component B (N=140). Squares = directions of samples; circles = msd with number of samples (N)≥3; triangles=msd with N≤2.

m and 22.2–23.9 m from the base (Fig. 8). The test was negative (test value=18.3 for a value at 95% confidence limit=6.6 and at 99% confidence limit=11.2). This is most likely due to contamination of component A on the normal directions (Fig. 6). The lack of conspicuous variation in structural attitude in the sedimentary succession prevented the application of the fold test.

The resultant in situ direction of component B, however, is totally dissimilar to any expected younger direction of magnetisation in this locality. The palaeopole corresponding to the structurally corrected B direction, however, is in very good agreement with that obtained in the nearby Winter Coast [2], and from volcanic rocks in Ukraine [3]. In addition, the dominant reverse polarity (Fig. 2) is in extremely good concordance with the polarity pattern interpreted for this time interval [17,18], and the change in polarity is stratigraphically controlled. This direction, therefore, is considered to represent the characteristic Ediacaran magnetisation which was acquired during or shortly after deposition of the rocks. While it may be argued that the directions obtained may have been affected by inclination shallowing, this is considered unlikely in the current situation given the lithologies involved and that similar coeval directions have been obtained from volcanic rocks [3].

In Table 2, all the statistical data from the sampling sites used in this study are listed. Site mean directions for component B were calculated using Fisher's [19] statistics and only in a few cases, did great circle analysis after [20] have to be employed (see Table 2). Approximately half of the site mean directions (Fig. 7b) were calculated from three or more specimens (circles) while the other half corresponds to mean directions calculated from two or less specimens (triangles).

For component A, the VGPs were calculated for each specimen, and for component B, the corresponding VGPs were calculated for each sampling level using

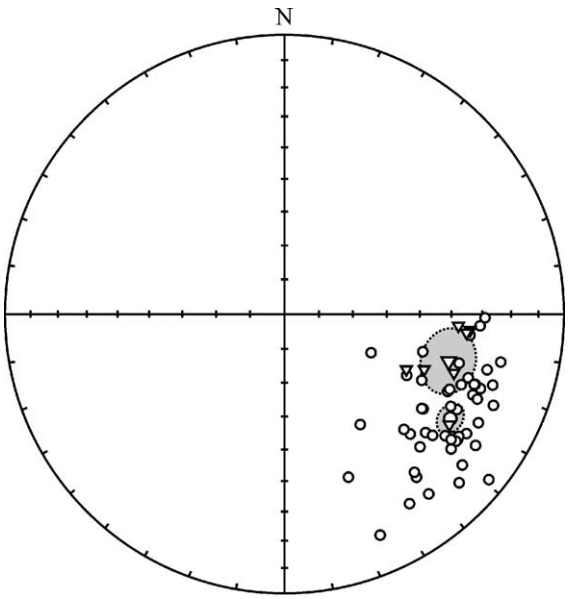

Fig. 8. The reversal test in Component B was performed using only "stable" directions (N=57) (intervals 16.3–17.7 m; 19.6–20.0 m; 22.2–23.9 m from the base, in Fig. 2). The test [16] was negative due to the contamination with component A. Big circle = mean direction of reverse polarity; big triangle = mean direction from normal polarity shown in the opposite direction.

Table 2
Site mean palaeomagnetic data from Zolotica

Site	Colour	n/N	J_r (A/m)	ChRM	α_{95}	k	VGP	Demagn.	Tilt cor.
				D_t, I_t			Long E, Lat N		Strike, dip
5 (base)	Red-green clay	3/3	$7.6\ 10^{-4}$	124.3, −39.7	10.7°	–	108°, −34.3°	Th 500–640 (GC)	172, 9
6	Red-green clay	4/4	$1.9\ 10^{-3}$	115.7, −44.7	14.3°	–	118.6°, −34.4°	Th 660–685 (GC)	"
7	Red-green clay	3/3	$2.4\ 10^{-3}$	115.3, −35.7	3.7°	1096.6	115.6°, −28.3	Th 620–700	"
8	Green clay	2/1	$1.2\ 10^{-3}$	124.5, −18.2	–	–	102°, −22.2°	AF 100–200	"
9	Red clay	3/2	$3.8\ 10^{-3}$	113.6, −19.5	–	–	113°, −18.8	Th 620–670	"
10	Grey f. sand	8/4	$2.3\ 10^{-3}$	110.8, −25.9	13.6°	46.3	117°, −21°	Th 610–690	"
12	Red-green clay	3/3	$2.8\ 10^{-3}$	109.1, −31	–	–	120°, −23°	Th 620–680	"
13	Red clay	4/4	$3.9\ 10^{-3}$	130, −34.5	12.3°	57	100.4°, −33.2°	Th 630–675	"
14	Red-green clay	3/3	$3.1\ 10^{-3}$	118.9, −30.1	9.7°	161.4	110.4°, −26.4°	Th 590–660	"
11	Grey f. sand	4/4	$2.2\ 10^{-3}$	105.6, −35.4	7.8°	248	124.7°, −24.2°	Th 590–685	"
16	Red clay	4/2	$3.4\ 10^{-3}$	126.2, −26.9	–	–	102.3°, −27.4°	Th 660–700	"
17	Green f. sand	4/2	$6.2\ 10^{-4}$	124.5, −40.2	–	–	108°, −34.7°	AF 140–200	"
18	Red clay	4/4	$2.3\ 10^{-3}$	110.2, −28.1	9.3°	99.5	118.2°, −22°	Th 590–675	"
19	Red clay	3/3	$1.6\ 10^{-3}$	105.3, −25.8	6.5°	356.7	122.2°, −18.7°	Th 650–675	"
21	Red-green f. sand	8/5	$4.2\ 10^{-3}$	113.2, −27.5	11.3°	46.6	115.2°, −22.8°	Th 640–680	"
20	Red clay	4/4	$4.1\ 10^{-3}$	113.8, −25.6	7.8°	141	114°, −22°	Th 665–685	"
22-0-2	Green f. sand	5/2	$6.6\ 10^{-4}$	134.4, −32.7	–	–	95.3°, −33.6°	AF 160–200	"
22-0-1	Green f. sand	5/2	$6.6\ 10^{-4}$	133.6, −37.9	–	–	97.7°, −36.6°	Th 600–650	"
23	Red clay	3/3	$4.2\ 10^{-3}$	127.1, −28.7	12.0°	106.1	101.8°, −28.7°	Th 660–680	"
24	Red clay	4/4	$4.7\ 10^{-3}$	108.8, −22.4	12.2°	57.7	118°, −18.3°	Th 620–675	"
25	Red clay	3/3	$4.6\ 10^{-3}$	119, −32.5	10.4°	142.2	111, −28°	Th 650–675	"
26	Red clay	4/2	$4.8\ 10^{-3}$	110.3, −28.5	–	–	118.2°, −22°	Th 660–675	"
27	Red clay	3/3	$4.3\ 10^{-3}$	126, −24.5	6.8°	328.1	102°, −26°	Th 640–670	"
28	Red f. sand	4/2	$2.8\ 10^{-3}$	123.3, −23.1	–	–	104.3°, −23°	Th 630–680	"
29	Red clay	3/3	$6.4\ 10^{-3}$	125, −24.8	12.7°	94.6	103°, −25.8	Th 590–670	"
32,38	Red clay	12/1	$8.6\ 10^{-3}$	137.3, −21.4	–	–	89.6°, −28.2	Th 660–680	"
33,39,40	Red clay	10/6	$5.4\ 10^{-3}$	121.5, −13.7	11.9°	32.4	104°, −19°	Th 650–680	"
34-0-2	Red-green clay	8/2	$7.5\ 10^{-4}$	106.2, −14.4	–	–	118.7°, −13.3°	Th 605–675	"
34-0-1	Red-green clay	8/2	$1.5\ 10^{-3}$	100.4, −28.4	–	–	127.4°, −13.3°	Th 600–670	"
41	Red clay	3/3	$1.4\ 10^{-2}$	94.3, −20.9	12.3	101.5	131°, −11.6°	Th 620–680	"
46	Red f. sand	3/3	$5.1\ 10^{-3}$	129.4, −19.2	11.2°	121.5	97.3°, −24.5°	Th 660–680	"
44,47	Red f. sand	5/5	$4.4\ 10^{-3}$	128.1, −17	8.7°	78	98°, −23°	Th 660–680	"
43	Red f. sand	3/3	$8.8\ 10^{-3}$	140.3, −11.2	12.9°	92.5	84.6°, −24°	Th 650–690	"
35,45	Red clay	6/2	$6.1\ 10^{-3}$	145.6, −6.6	–	–	78.3°, −23°	Th 640–670	"
37	Red clay	3/2	$4.1\ 10^{-3}$	100.5, −8.2	–	–	122.6°, −8°	Th 660–690	"
48	Red clay	3/3	$5.5\ 10^{-3}$	131.9, −8.3	13.1°	90.2	92.7°, −20°	Th 650–675	"
49	Red clay	3/3	$4.8\ 10^{-3}$	139.7, −2.3	9.6°	166.1	83.8°, −19.5°	Th 650–675	"
50	Red-green clay	3/3	$5.8\ 10^{-3}$	138.1, −17.6	2.3°	2979	88°, −26.5°	Th 630–675	"
51	Red clay	3/3	$6.1\ 10^{-3}$	132.6, −13.1	12.8°	93.6	92.8°, −22.5°	Th 650–710	"
52	Red clay	3/3	$7.5\ 10^{-3}$	123, −22.1	12.0°	107.4	104.3°, −23.7°	Th 630–680	"
53	Red clay	3/2	$6.8\ 10^{-3}$	116.8, −5.4	–	–	106.8°, −13.2°	Th 650–670	"
54	Red clay	3/3	$5.3\ 10^{-3}$	120.9, −11.1	8.6°	205.4	104°, −17.5°	Th 610–680	"
55	Red-green clay	3/2	$3.6\ 10^{-3}$	128.9, −7.5	–	–	95.5°, −18.6°	Th 605–660	"
56	Red clay	3/3	$1.1\ 10^{-2}$	121.4, −31.5	13.1°	89.5	108.3°, −28.2°	Th 640–700	"
57	Red clay	4/4	$1.2\ 10^{-2}$	105, −30.2	12.9°	51.3	123.7°, −21°	Th 650–675	"
58	Red clay	3/3	$1.3\ 10^{-2}$	108.4, −31	14.1°	77.1	120.7°, −22.8°	Th 660–670	"
59	Red clay	3/3	$1.2\ 10^{-2}$	96.8, −37.1	13.4°	85.3	133.3°, −21.6°	Th 640–680	"
60	Red clay	3/2	$1.2\ 10^{-2}$	119.9, −38.1	–	–	112°, −31.6°	Th 665–680	"
61	Green clay	6/1	$4.2\ 10^{-4}$	107.4, −18.4	–	–	118.5°, −15.7°	Th 500–580	"
63	Red-green clay	4/1	$3.0\ 10^{-3}$	91.5, −13.3	–	–	132°, −6.8°	Th 665–675	"
64	Red clay	3/3	$4.9\ 10^{-3}$	68.5, −18.1	12.8°	–	153.8°, 0.1°	Th 640–685 (GC)	"
65	Red clay	4/2	$6.4\ 10^{-3}$	71.6, −21.2	–	–	151.7°, −2.6°	Th 665–680	"
66	Red-green f. sand	2/1	$2.4\ 10^{-3}$	72, −24.6	–	–	152°, −4.5°	Th 670–675	"
70	Red clay	3/1	$6.0\ 10^{-3}$	211.5,48.1	–	–	13°, 7.8°	Th 605–635	"
74	Red clay	3/2	$3.2\ 10^{-3}$	228.2, 56.5	–	–	1.5°, 19.2°	Th 580–660	"
75	Red clay	9/5	$4.9\ 10^{-3}$	273.8, 37.7	10.2°	56.8	316.2°, 20.7°	Th 630–675	"

(continued on next page)

Table 2 (*continued*)

Site	Colour	n/N	J_r (A/m)	ChRM	α_{95}	k	VGP	Demagn.	Tilt cor.
				D_t, I_t			Long E, Lat N		Strike, dip
77	Red-green f. sand	5/4	$3.8\ 10^{-3}$	275, 33.8	10.9°	71.8	314°, 19°	Th 665–680	"
79	Red clay	2/1	$2.1\ 10^{-3}$	294.3, 50.4	–	–	302.7°, 38°	Th 635–660	"
80	Red clay	4/3	$2.9\ 10^{-3}$	275.8, 34.9	14.0°	78.3	313.5°, 19.8°	Th 640–670	"
81	Red clay	3/3	$3.8\ 10^{-3}$	303.9, 29.7	9.4°	174.3	285.3°, 28°	Th 640–670	"
82	Red-green clay	3/2	$4.4\ 10^{-3}$	291.6, 45.3	–	–	302.8°, 33°	Th 630–660	"
85	Green c. sand	3/1	$5.4\ 10^{-4}$	154.6, −12.4	–	–	69.4°, −28°	AF 50–60	"
86	Red-green m. sand	3/1	$1.6\ 10^{-3}$	132.6, −40.0	–	–	99.5°, −37.6°	Th 675–685	"
96	Red m. sand.	4/2	$3.3\ 10^{-3}$	151.1, −6.8	–	–	72.5°, −24.5°	Th 665–680	"
97	Red c. sand	3/1	$3.0\ 10^{-3}$	107.9, −43.3	–	–	125.4°, −30.2°	Th 640–650	"
99	Red c. sand	3/1	$2.2\ 10^{-3}$	68.5, −36.8	–	–	158.2°, −10.2°	Th 665–680	"
104	Red m. sand	6/2	$2.6\ 10^{-3}$	46.4, −29.0	–	–	176.2°, 1.8°	Th 670–680	"
110	Green m. sand	4/2	$9.2\ 10^{-4}$	108.4, −52.1	2.7°	–	129.2°, −37°	AF 30–70 (GC)	"
106	Red f. sand	5/1	$2.8\ 10^{-3}$	111.0, −25.6	–	–	116.8°, −21°	Th 670–675	"
107-0-2	Red f. sand	8/2	$2.9\ 10^{-3}$	95.0, −37.0	–	–	135°, −20.8°	Th 650–680	"
107-0-1	Red f. sand	8/2	$3.0\ 10^{-3}$	117.0, −19.9	–	–	109.7°, −20.3°	Th 650–680	"
108-0-3	Red f. sand	3/2	$2.7\ 10^{-3}$	107.2, −30.5	–	–	121.7°, −22°	Th 630–680	"
108-0-2	Red f. sand	3/2	$3.8\ 10^{-3}$	113.4, −35.6	–	–	117.4°, −27.5°	Th 630–680	"
108-0-1	Red f. sand	8/2	$3.5\ 10^{-3}$	127.2, −35.5	–	–	103.6°, −32.8°	Th 650–680	"
111-0-2	Red f. sand	6/3	$4.4\ 10^{-3}$	123.5, −24.2	8.9°	–	104.3°, −25°	Th 590–665 (GC)	"
111-0-1	Red f. sand	6/1	$3.0\ 10^{-3}$	108.2, −15.3	–	–	117°, −14.6°	Th 630–675	"
112-0-2	Red clay	5/1	$3.7\ 10^{-3}$	168.5, −37.3	–	–	55.7°, −44.6°	Th 670–675	"
112-0-1	Red clay	5/2	$5.0\ 10^{-3}$	153.8, −48.5	–	–	77.6°, −50.4°	Th 670–690	"
109-0-1	Red clay	8/1	$3.5\ 10^{-3}$	171.3, −15.9	–	–	50.7°, −32.2°	Th 665–675	"
118-0-2	Red c. sand	2/1	$3.3\ 10^{-3}$	116.5, −23.8	–	–	111°, −22°	Th 670–680	96, 5
119	Red c. sand	5/2	$2.7\ 10^{-3}$	104.7, −34.6	7.5°	–	125.3°, −23.3°	Th 660–675 (GC)	"
121	Red m. sand	4/1	$4.4\ 10^{-3}$	157.0, −18.8	–	–	67.5°, −31.8°	Th 675–685	"
122	Red c. sand	5/2	$3.5\ 10^{-3}$	117.4, −9.6	–	–	107°, −15.4°	Th 630–660	"
123	Red c. sand	5/1	$3.2\ 10^{-3}$	147.2, −17.2	–	–	78.2°, −28.8°	Th 660–670	"
124	Red m. sand	3/1	$2.2\ 10^{-3}$	119.3, −21.6	–	–	108°, −22°	Th 660–680	"
131	Green m. sand	5/2	$1.1\ 10^{-3}$	93.4, −30.6	–	–	134.4°, −16.4°	AF 70–150	"
133	Green f. sand	5/1	$8.9\ 10^{-4}$	141.0, −25.9	–	–	86.5°, −31.8°	Th 660–665	"
134	Red f. sand	3/2	$2.5\ 10^{-3}$	146.6, −19.8	–	–	79.2°, −30°	Th 590–640	"
135-0-2	Red f. sand	5/2	$2.8\ 10^{-3}$	96.4, −33.6	–	–	132.6°, −19.3°	Th 640–680	"
135-0-1	Red f. sand	5/2	$3.0\ 10^{-3}$	126.6, −24.6	–	–	101.3°, −26.3°	Th 640–670	"
136	Red f. sand	9/1	$2.8\ 10^{-3}$	140.6, −27.6	–	–	87.3°, −32.6°	Th 650–670	"
139	Red f. sand	6/3	$4.1\ 10^{-3}$	111.8, −32.4	11.4°	117.9	118°, −25°	Th 650–670	"
140	Red clay	5/4	$4.6\ 10^{-3}$	91.0, −29.0	13.7°	46.2	136°, −14.5°	Th 650–680	"
141	Red clay	6/4	$6.6\ 10^{-3}$	127.0, −26.3	12.9°	51.8	101.3°, −27.4°	Th 650–670	"
142	Red f. sand.	16/2	$2.6\ 10^{-3}$	114.4, −35.3	–	–	116.3°, −27.7°	Th 640–670	"
143	Red-green f. sand	8/2	$2.3\ 10^{-3}$	158.6, −37.4	–	–	68.4°, −43.2°	Th 640–670	"
144	Red m. sand	3/2	$2.0\ 10^{-3}$	129.3, −32.0	–	–	100.4°, −31.4°	Th 590–660	"
146	Red m. sand	3/1	$5.5\ 10^{-3}$	130.3, −17.7	–	–	96°, −24°	Th 660–675	"
147	Red f. sand	4/2	$2.7\ 10^{-3}$	134.0, −40.3	–	–	98°, −38.3°	Th 650–680	"
148	Red f. sand	3/3	$3.7\ 10^{-3}$	141.3, −18.6	13.3°	–	84.8°, −28°	Th 650–670 (GC)	"
149	Red f. sand	12/3	$1.6\ 10^{-3}$	160.5, −62.1	13.0°	–	76°, −65.3°	Th 500–650 (GC)	"
150-0-2	Red f. sand	6/2	$1.4\ 10^{-3}$	113.9, −62.2	–	–	132°, −48.4°	Th 590–650	"
150-0-1	Red f. sand	7/2	$1.2\ 10^{-3}$	102.5, −21.8	–	–	123.8°, −15.4°	Th 590–665	"
151-0-2	Red f. sand	4/1	$2.2\ 10^{-3}$	129.0, −6.6	–	–	95.3°, −18.2°	Th 590–665	"
151-0-1	Red f. sand	5/1	$2.3\ 10^{-3}$	134.0, −14.1	–	–	91.6°, −23.5°	Th 590–665	"
154	Red-green m. sand	3/2	$2.8\ 10^{-3}$	129.0, −24.3	–	–	98.8°, −27°	Th 640–665	"
155	Green f. sand.	3/1	$4.0\ 10^{-4}$	156.6, −14.9	–	–	67.5°, −29.7°	AF 70–100	"
157	Green f. sand	3/1	$5.0\ 10^{-4}$	145.5, −50.4	–	–	89°, −49.7°	Th 650–675	"
160	Red clay	3/3	$2.2\ 10^{-3}$	158.9, −61.5	10.8°	131.6	78°, −64.2°	Th 660–680	"
162	Green f. sand	15/3	$1.2\ 10^{-3}$	116.6, −49.5	13.1°	89.9	120°, −38.3°	Th 610–685	"
161-0-1	Red-green f. sand	4/3	$2.1\ 10^{-3}$	105.1, −47.5	13.5°	84.8	129.8°, −32°	Th 600–680	"
163	Red-green clay	3/3	$3.8\ 10^{-3}$	125.0, −65.0	8.8°	198.1	125°, −56°	Th 630–685	"
164	Red-green f. sand	6/6	$3.0\ 10^{-3}$	131.7, −70.1	8.0°	70.3	127.8°, −64°	Th 630–680	"

Table 2 (*continued*)

Site	Colour	n/N	J_r (A/m)	ChRM	α_{95}	k	VGP	Demagn.	Tilt cor.
				D_t, I_t			Long E, Lat N		Strike, dip
165	Red clay	4/3	$3.9\ 10^{-3}$	113.1, −28.5	5.5°	498.8	115.6°, −23.3°	Th 650–670	"
166	Red clay	4/4	$3.0\ 10^{-3}$	128.6, −51.3	7.3°	159.1	108.8°, −44.5°	Th 665–680	"
167	Red clay	3/3	$3.1\ 10^{-3}$	159.1, −38.8	11.6°	114.3	68°, −44.2°	Th 590–640	"
168	Red clay	5/5	$2.4\ 10^{-3}$	146.5, −64.3	4.6°	279.2	99.6°, −63.5°	Th 640–680	"
169	Red clay	4/3	$2.7\ 10^{-3}$	137.5, −68.1	13.9°	79.3	117.4°, −64.2°	Th 665–680	"
170	Red-green clay	4/4	$2.8\ 10^{-3}$	121.5, −60.3	13.1°	50.3	123°, −49.7°	Th 630–680	"
171	Red clay	4/2	$4.7\ 10^{-3}$	109.8, −30.8	–	–	119.4°, −23.2°	Th 630–680	"
172	Red-green clay	3/2	$2.7\ 10^{-3}$	131.1, −36.8	–	–	100°, −35°	Th 630–675	"
173	Red-green clay	4/3	$2.0\ 10^{-3}$	132.1, −43.8	4.9°	626.5	101.4°, −40°	Th 640–660	"
174	Red-green clay	3/3	$2.5\ 10^{-3}$	125.9, −41.2	9.4°	172.6	107°, −36°	Th 630–675	"
175	Red-green clay	4/4	$2.1\ 10^{-3}$	126.8, −58.7	10.0°	85.2	116°, −50.3°	Th 610–675	"
176	Red-green clay	4/3	$2.4\ 10^{-3}$	148.0, −57.6	13.1°	89.0	90.4°, −57°	Th 670–680	"
177	Red-green clay	6/5	$2.9\ 10^{-3}$	143.5, −53.0	9.4°	143.5	93°, −51.3°	Th 650–670	"
180	Red-green clay	5/5	$5.9\ 10^{-3}$	154.0, −26.4	11.5°	44.9	72°, −35.4°	Th 640–670	"
181	Red-green clay	4/4	$4.4\ 10^{-3}$	149.9, −26.6	13.1°	50.4	76.7°, −34.6°	Th 630–675	"
182.1-2	Red clay	2/2	$2.6\ 10^{-3}$	155.9, −47.8	–	–	74.6°, −50.4°	Th 630–680	"
182.3-2	Red clay	2/2	$1.4\ 10^{-2}$	161.0, −32.6	–	–	64.6°, −40.5°	Th 630–680	"
182.3-1	Red clay	6/4	$1.1\ 10^{-2}$	163.8, −44.7	5.8°	247.8	63°, −49.4°	Th 630–680	"
183	Red clay	6/3	$2.2\ 10^{-2}$	186.9, −33.4	3.9°	1022.4	31.6°, −42.4°	Th 630–680	"
184	Red f. sand	4/4	$1.5\ 10^{-2}$	223.7, −20.0	9.6°	93.5	350.7°, −27.2°	Th 630–680	"
185	Red clay	4/4	$1.2\ 10^{-2}$	222.2, −20.3	9.8°	88.9	352.2°, −27.8°	Th 630–680	"
186	Red clay	3/1	$4.3\ 10^{-3}$	117.4, −22.3	–	–	110°, −21.7°	Th 665–670	"
187	Red clay	3/2	$4.7\ 10^{-3}$	226.1, −52.7	–	–	337.1°, −47.7°	Th 630–670	"
189	Red clay	2/1	$7.8\ 10^{-3}$	188.9, −4.0	–	–	30.6°, −26.1°	Th 640–680	"
188	Red clay	1/1	$8.8\ 10^{-3}$	190.8, −32.4	–	–	26.7°, −41.5°	Th 650–680	"
190 (top)	Red clay	1/1	$3.0\ 10^{-2}$	143.7, −16.5	–	–	81.8°, −27.6°	Th 650–680	"

Symbols: n/N=total samples/selected samples; J_r: natural remanent magnetization intensity; ChRM: characteristic remanent magnetization; D_t, I_t: declination, inclination after tilt correction; α_{95}: semi-angle of confidence; k: Fisher's precision parameter; VGP: virtual geomagnetic pole; Demagn.: demagnetization range in mT (AF) or °C (thermal); GC: great circles. Tilt correction: strike follows the right-hand rule.

only the site mean directions which are clearly fully normal or inverse in polarity (Fig. 2). The corresponding palaeomagnetic poles were then calculated from the VGP data for the two different magnetisations (Table 3). For component A the in situ palaeo-south pole is located at: Lon=55.4 °E, Lat=30.9 °N, A_{95}=2.7°, N=575, and the pole for the primary component B direction is situated at: Lon=109.9 °E, Lat=28.3 °S, A_{95}=3.8°, N=57.

6. Discussion

The most generally adopted APW path for Baltica in Ediacaran to Early Ordovician times is that of Torsvik et al. [1], Smethurst et al. [21] and Torsvik and Rehnström [22]. However, as discussed by Meert et al. [23], Popov et al. [2] and Khramov et al. [24], this sector of the APW is based on a rather sparse dataset, some of which are of questionable reliability. For Cryogenian–Early Ediacaran times, this path is anchored by the well constrained 750 Ma palaeopoles situated in South Africa (present day co-ordinates) and (Table 4) by the 650 Ma Egersund palaeopoles located in Arabia. The Ediacaran sector on the other hand, is defined by the approximately 580 Ma Sredny, and Komagnes and Fen poles (given the new age dates for the Fen complex in [23] which form essentially two groups separated by some 70° of longitude located in NW Russia. Due to the lack of palaeomagnetic data, the Cambrian sector was defined by interpolation between

Table 3
Mean directions and corresponding palaeomagnetic poles of components A and B at Zolotica

Component	Age	Mean directions Dec°, Inc°	N	α_{95}	Plat (°)	Plon (°)	A_{95}
A (in situ)	E. Ordovician?	157.1, 68.0	575	1.9	31.0	55.4	2.7
B (bedding-corr.)	Vendian	120.3, −31.7	57	3.9	−28.3	110	3.8

N=number of samples; Dec, Inc: declination, inclination; α_{95}: semi-angle of confidence; k: Fisher's precision parameter.

Table 4
Other palaeomagnetic poles mentioned in this study

Rock unit	Age (Ma)	Lat. N	Long. E	A_{95} (dp/dm)	Reference
Egersund Dykes	650	28.0	52.0	11.5	[35]
Egersund Dykes	650	22.0	51.0	14.0	[36]
Nyborg Fm.	653 ± 7	24.3	88.5	*17/25*	[25]
Sredny Dyke	580	73.0	95.0	2.3	[32]
Komagnes Dyke	580	63.0	103.0	4.5	[32]
Fen Complex	583 ± 15	56.0	150.0	*7/10*	[23]
Torneträsk Fm.	545–530	56.0	116.0	*12/15*	[22]

the 580 Ma poles and the well defined Early Ordovician pole situated in Arabia. More recent data from Early Cambrian rocks of N Norway allow refinement with a well constrained pole [22] which plots on the Early Cambrian segment of the path proposed by Torsvik et al. [1]. Given questions concerning age constraints for the Komagnes and Sredny group of palaeopoles, however, Torsvik and Rehnström [22] used the most recent Fen complex data [23] to anchor the Ediacaran APW path. Reliability of the Fen complex data themselves, however, have also been questioned by the original authors and subsequently by Popov et al. [2], with suggestion that they represent a younger remagnetisation event (taking the opposite polarity option).

In contrast, taking into consideration the data presented here and other poles which are either more recently published or not taken into account by Torsvik and coauthors, there is an increasingly large data set for Late Neoproterozoic to Cambrian times that fall consistently away from this APW path. These data include the (Table 4) 653 ± 7 Ma Nyborg pole [25], the (Table 5) 589 Ma [26] Alnø pole [27], the approximately 555 Ma poles from Zolotica and the Winter Coast (this study and [2]) and Ukraine [3], the Ediacaran Stappogiedde data [28], the 510 ± 20 Ma Scandinavian Caledonides (SC) pole [29] and the Late Cambrian Narva River pole [24]. The Late Cryogenian Nyborg data, which are constrained by a positive fold test, were considered by the original authors as primary in origin. However, the pole is very similar to the Latest Cambrian SC pole (constrained by a positive contact test) and the Narva River pole (based only on 14 samples, but with a positive reversal test), thus suggesting that the Nyborg data may represent a pre-folding Cambrian overprint. The Late Ediacaran poles from Alnø, Zolotica, the Winter Coast and Ukraine form a fairly well grouped cluster of poles which are completely distinct from any possible younger remagnetisation or combination of remagnetisations directions. Taking all the Late Neoproterozoic poles into consideration (pole numbers 8 to 13; Table 5), a mean pole position for the Upper Ediacaran of Lon = 127.1°E, Lat = 28.7 ± S, A_{95} = 13.8°, N = 6, is obtained. This plots some considerable distance from the Ediacaran Fen complex and Sredny/Komagnes data. They are also supported by the less well constrained Late Ediacaran Upper Stappogiedde data of Bylund [28] which consist of single-site derived VGPs (triangles in Fig. 9).

Table 5
South palaeopoles from Baltica of Cryogenian (750 Ma) to Early Ordovician (480 Ma) ages used in Fig. 9

Rock unit/locality	Lithology	Age (Ma)	Lat. N	Long. E	A_{95} (dp/dm)	Reference
1. Sredny–Kildin	Sediments	750	−30.0	16.0	*6/12*	[30]
2. Kola Peninsula Mean Pole	Sediments	750	−28.6	17.2	7.5	[31]
3. Kildinskaya Fm.	Sediments/dykes	750	−26.0	13.0	*4/7*	[32]
4. Vadsø Group	Sediments	750	−24.0	27.0	*5/11*	[33]
5. Stappogiedde Fm. (site 5)	Sediments	E. Ediacaran	−16.0	39.0	*7/15*	[28]
6. Stappogiedde Fm. (site 6)	Sediments	E. Ediacaran	−1.0	78.0	*6/11*	[28]
7. Alnø Complex	Intrusives	589	−8.0	92.0	*5/9*	[27]
8. Zolotica 1	Sediments	~556	−32.0	113.0	*2/3*	[34]
9. Zolotica 2	Sediments	~556	−28.3	110.0	3.8	This study
10. Stappogiedde Fm. (site 9)	Sediments	L. Ediacaran	−36.0	131.0	*10/13*	[28]
11. Winter Coast	Sediments	555 ± 3	−25.3	132.2	*2/4*	[2]
12. Rafalivka	Volcanics/sediments	555 ± 5	−36.0	153.0	*3/4*	[3]
13. Stappogiedde Fm. (site 7)	Sediments	L. Ediacaran	−10.0	126.0	*8/15*	[28]
Upper Vendian (average)	Sediments	550 ± 5	−28.7	127.1	13.8	This study
14. Scad. Caled.	Intrus./metamorph.	510 ± 20	31.0	86.0	*11/15*	[29]
15. River Narva 1	Sediments	500	22.0	86.7	*4.5/6.5*	[24]
16. River Narva 2	Sediments	480	18.0	54.6	*6/8*	[24]
17. Zolotica-comp. A	Sediments	E. Ordovician?	31.0	55.4	2.7	This study

A_{95} (dp/dm): confidence limits of the pole.

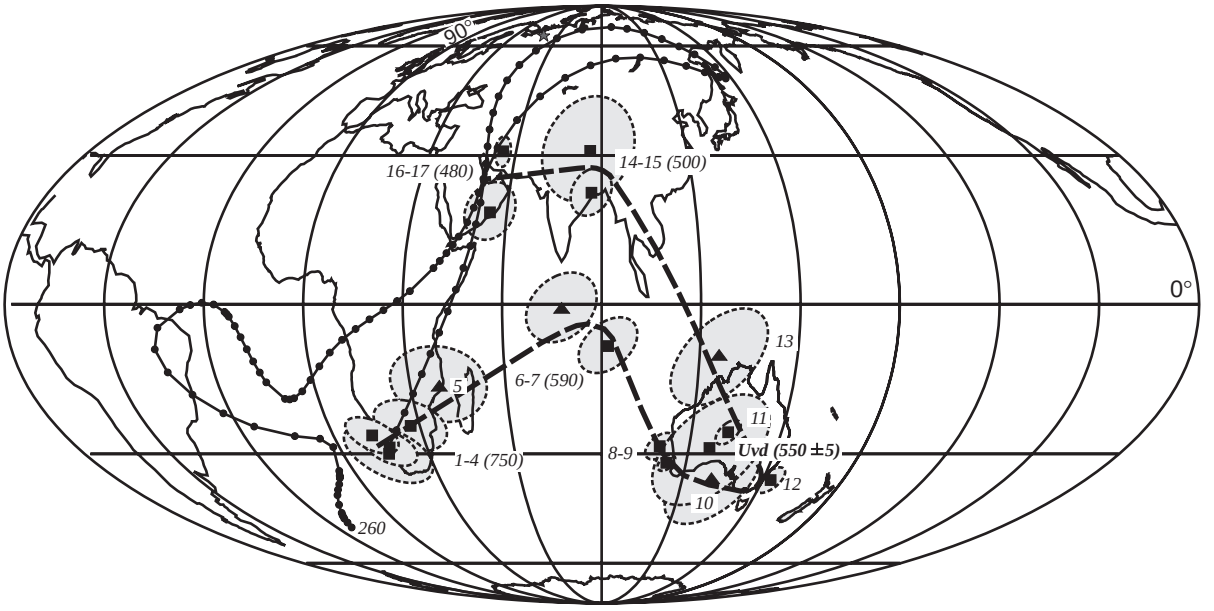

Fig. 9. Baltica's APW paths proposed by Torsvik et al. [1] (solid line) and in this paper (dashed line) for Cryogenian (~750 Ma) to Ordovician (~480 Ma) times. After 750 Ma, the palaeopoles located over South Africa (p.d.c.) moved to the east until they reached Australia at ~555 Ma and remained more or less in the same position until ~545 Ma (Ediacaran–Cambrian boundary). Subsequently they moved to the northwest until at ~480 Ma they reached the Arabian Peninsula. Star = sample locality; squares = palaeomagnetic poles; triangles = virtual geomagnetic poles (one sampling site). Poles 1–17 = see Table 5.

Thus, given the new data presented here, and considering the questions concerning the age of the Sredny, Komagnes and Fen data, there is now a fairly compelling argument that the Late Ediacaran mean pole presented here, should be used to anchor the APW path of Baltica. Given the rather sparse data set for the Neoprotoerozoic of Baltica as a whole, one of the main problems in construction of the APW path is which polarity option to choose for the poles. As the data stand, it is not possible to determine whether the normal or reverse option should be taken for the new Late Ediacaran mean pole presented here (Fig. 10). The path shown here has been constructed using the reverse polarity option (C1), in agreement with the path presented by Popov et al. [2] According to this new APW path for Baltica, the Zolotica sampling locality was situated close to the equator from Cryogenian through to the Early Late Ediacaran, moving gradually to the south at a rate of c. 1 cm/yr. This was followed by a sharp shift in the motion of the plate toward the north at about 8 cm/yr until it positioned at low to intermediate latitudes in the Late Ediacaran. Near the boundary with the Cambrian, Baltica moved back to the south at higher rates (c.13 cm/yr) and reached intermediate to high southern latitudes in the Early Ordovician.

This is a very tentative APW path, constructed in order to minimise large scale rotations of Baltica in the Late Neoproterozoic. However, it is generally accepted that Baltica remained in the southern hemisphere in the Neoproterozoic and early Palaeozoic which would clearly require inversion of the Late Ediacaran poles and necessitates large scale rotations of Baltica (C2, Fig. 10). In keeping with the southern hemispherical position of Baltica and to avoid high drift rates, Nawrocki et al. [3] chose the normal polarity option for their Late Ediacaran data. However, as described above, the drift rates implied by the path shown here are not high (13 cm/yr at most with C1, Fig. 10) and, furthermore, the normal polarity option also brings into question the polarities of the other Neoproterozoic poles for Baltica, and the sense of the rotations which are required. These problems of which poles should be inverted and the rotational history of Baltica cannot be resolved until more accurate and reliable palaeomagnetic data are available, and at this stage construction of a robust and unique Neoproterozoic/Cambrian APW path for Baltica is not possible.

7. Conclusions

High quality palaeomagnetic data and radiometric ages have been obtained from the Zolotica section. The rocks yield an age of ~556 Ma. (U/Pb SHRIMP

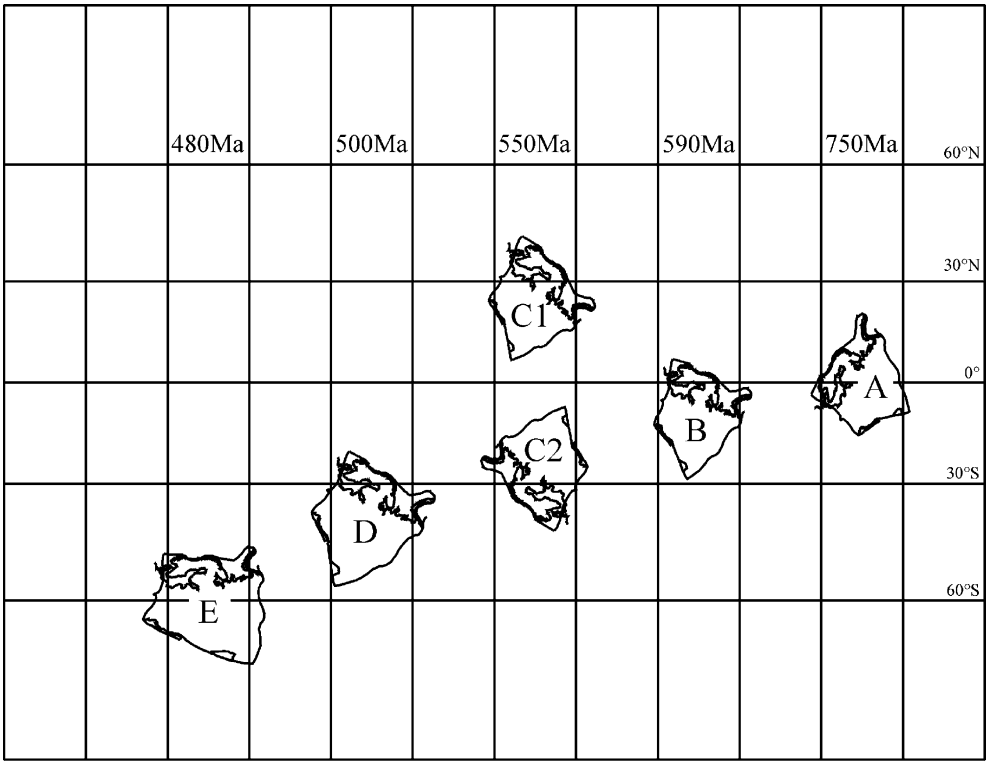

Fig. 10. Baltica's latitudinal positions between the Cryogenian and the Early Ordovician, calculated with the poles in Table 5. Baltica moved from a position near the Equator in the Cryogenian through to the Early Late Ediacaran toward the south at c.1 cm/yr. Subsequently, the plate shifted to the north (C1) in our reverse polarity option moving at c. 8 cm/yr or alternatively (C2), to the south in the normal polarity option proposed in [3], and positioned in low to intermediate latitudes. During the Early Cambrian, Baltica moved southward again at c.13 cm/yr until it situated in intermediate to high southern latitudes in the Early Ordovician.

method) and two magnetic components were isolated. Component A which is carried by magnetite yields a palaeopole situated at Long=55.4°E, Lat=30.9°N A_{95}=2.7°, N=575. Given that this plots directly on the Early Ordovician pole for Baltica, this component is considered to be secondary in character and possibly Early Ordovician in age. Component B is carried by haematite whose direction of magnetisation is fully discordant with any expected younger magnetisation directions for the Zolotica region and is interpreted as representing the primary magnetisation acquired at or soon after the deposition of the sediments in the Late Ediacaran. The corresponding palaeomagnetic pole is located at Long=110°E, Lat=28.3°S, A_{95}=3.8°, N=57. These data are in good agreement with previously published coeval data from NW Russia and Ukraine, thus supporting the APW paths presented by Popov et al. [2] and Nawrocki et al. [3], depending on the polarity option chosen, and are in marked contrast to the more traditional path proposed by Torsvik et al. [1], which these data clearly bring into question.

Acknowledgements

This project has been financed by the Deutsche Forschungsgemeinschaft. The authors also wish to thank Alfonso Fernández Davila for his great assistance and company in the field, and Maxim Alexyutin for his help regarding the geology. JAT also thanks financial support from the VWStiftung. The authors also acknowledge the valuable reviews of T.H. Torsvik and S. Pisarevsky, which were very helpful in improving the quality of the original manuscript.

References

[1] T.H. Torsvik, M.A. Smethurst, J.G. Meert, D.V.R. Van, W.S. McKerrow, M.D. Brasier, B.A. Sturt, H.J. Walderhaug, Continental break-up and collision in the Neoproterozoic and Palaeozoic — a tale of Baltica and Laurentia, Earth Sci. Rev. 40 (1996) 229–258.

[2] V. Popov, A. Iosifidi, A. Khramov, J. Tait, V. Bachtadse, Paleomagnetism of Upper Vendian sediments from the Winter Coast, White Sea region, Russia: implications for the paleogeography of

Baltica during Neoproterozoic times, J. Geophys. Res. 107 (B11) (2002), doi:10.1029/2001JB001607 (EPM 10-1 to EPM 10-8).
[3] J. Nawrocki, A. Boguckij, V. Katinas, New Late Vendian palaeogeography of Baltica and the TESZ, Geol. Q. 48 (4) (2004) 309–316.
[4] V.S. Shchukin, S.M. Sablukov, V.K. Sobolev, V.A. Larchenko, A.I. Makhin, Geology of diamond deposits in the Arkhangelsk region of Russia, Trans. Soc. Min. Metall. Explor. Inc. 300 (1996) 20–27.
[5] V.S. Shchukin, S.M. Sablukov, L.I. Sablukova, E.A. Belousova, W.L. Griffin, Late Vendian aerial alkaline volcanism of rift type in the Zimny Bereg kimberlite area (Arkhangelsk diamondiferous province), Deep-seated Magmatism, Magmatic Sources and the Problem of Plumes, 2002, pp. 203–212.
[6] I.S. Williams, U–Th–Pb geochronology by ion microprobe, in: M.A. McKibben, W.C. Shanks III, W.I. Ridley (Eds.), Applications of Microanalytical Techniques to Understanding Mineralizing Processes, Rev. Economic Geol., vol. 7, 1998, pp. 1–35.
[7] K.R. Ludwig, SQUID 1.00, A User's Manual, Berkeley Geochronology Center Special Publication, vol. 2, 2000 2455 Ridge Road, Berkeley, CA 94709, USA.
[8] L.P. Black, S.L. Kamo, TEMORA 1: a new zircon standard for U–Pb geochronology, Chem. Geol. 200 (2003) 155–170.
[9] G.W. Wetherill, Discordant uranium–lead ages, Trans. Amer. Geophys. Union 37 (1956) 320–326.
[10] K.R. Ludwig, User's Manual for Isoplot/Ex, Version 2.10, A geochronological Toolkit for Microsoft Excel, Berkeley Geochronology Center Special Publication, vol. 1a, 1999 2455 Ridge Road, Berkeley CA 94709, USA.
[11] J. Andersson, U. Söderlund, D. Cornell, L. Johansson, C. Möller, Sveconorwegian–Grenvillian deformation, metamorphism and leucosome formation in SW Sweden, SW Baltic Shield: constraints from a Mesoproterozoic granite intrusion, Precambrian Res. 98 (1999) 151–171.
[12] H. Downes, P. Peltonen, I. Manttari, E.V. Sharkov, Proterozoic zircon ages from lower crustal granulite xenoliths, Kola Peninsula, Russia; evidence for crustal growth and reworking, Geol. Soc. London 159 (5) (2002) 485–488.
[13] B. Bingen, O. Nordgulen, E.M.O. Sigmond, R. Tucker, J. Mansfeld, K. Hgdahl, Relations between 1.19–1.13Ga continental magmatism, sedimentation and metamorphism, Sveconorwegian province, S Norway, Precambrian Res. 124 (2003) 215–241.
[14] T. Andersen, Detrital zircons as tracers of sedimentary provenance: limiting conditions from statistics and numerical simulation, Chem. Geol. 216 (2005) 249–270.
[15] J.L. Kirschvink, The least-squares line and plane and the analysis of palaeomagnetic data, Geophys. J. R. Astron. Soc. 62 (1980) 699–718.
[16] P. McFadden, M.W. McElhinny, Classification of the reversal test in paleomagnetism, Geophys. J. Int. 103 (1990) 725–729.
[17] G.V.S. Poornachandra Rao, M.S. Bhalla, Magnetostratigraphy of Vindhyan Supergroup, J. Geol. Soc. India 47 (1996) 29–32.
[18] O.N. Tretyak, L.I. Vigilyanskaya, A. Ya. Karzanova, Vendian paleomagnetism of Ukraine (problem of the boundary between the Precambrian and Phanerozoic Periods), Geophys. J. 16 (1997) 499–513.
[19] R.A. Fisher, Dispersion on a sphere, Proc. R. Soc. Lond., A 217 (1953) 295–305.
[20] P. McFadden, M.W. McElhinny, The combined analysis of remagnetization circles and direct observations in paleomagnetism, Earth Planet. Sci. Lett. 87 (1988) 161–172.
[21] M.A. Smethurst, A.N. Khramov, S. Pisarevsky, Palaeomagnetism of the Lower Ordovician Orthoceras Limestone, St. Petersburg, and a revised drift story for Baltica in the early Palaeozoic, Geophys. J. Int. 133 (1) (1998) 44–56.
[22] T.H. Torsvik, E.F. Rehnström, Cambrian palaeomagnetic data from Baltica: implications for true polar wander and Cambrian palaeogeography, J. Geol. Soc. (Lond.) 158 (2001) 321–329.
[23] J.A. Meert, T.H. Torsvik, E.A. Eide, S. Dahlgren, Tectonic significance of the Fen Province, S. Norway: constraints from geochronology and palaeomagnetism, J. Geol. 106 (1998) 553–564.
[24] A.N. Khramov, A.G. Iosifidi, V. Bachtadse, J. Tait. New palaeomagnetic results for the Early Palaeozoic of Baltica: implications for its Apparent Polar Wander Path, Geoph. J. Int. (submitted for publication).
[25] T.H. Torsvik, K.C. Lohmann, B.A. Sturt, Vendian glaciations and their relation to the dispersal of Rodinia: paleomagnetic constraints, Geology 23 (1995) 727–730.
[26] H.J. Walderhaug, T.H. Torsvik, E.A. Eide, J.G. Meert, Magnetic properties and age of the Aln½ Carbonatite Complex (Sweden), Geophys. Res. Abstr. EUG-EGS-AGU 5 (2003) 10358.
[27] J.D.A. Piper, Magnetic properties of the Alnø Complex, Geol. Fören. Stockh. Förh. 103 (1981) 9–15.
[28] G. Bylund, Palaeomagnetism of Vendian–Early Cambrian sedimentary rocks from E. Finnmark, Norway, Tectonophysics 231 (1994) 45–57.
[29] T.H. Torsvik, O. Olesen, P.D. Ryan, A. Trench, On the palaeogeography of Baltica during the Palaeozoic: new palaeomagnetic data from the Scandinavian Caledonides, Geophys. J. Int. 103 (1990) 261–279.
[30] S.V. Shipunov, N.M. Chumakov, Palaeomagnetism of Upper Proterozoic deposits of the Kola Peninsula, Geotectonics 25 (5) (1991) 401–410.
[31] A.N. Khramov, Paleomagnetic directions and pole positions, data for the USSR No. 6, Materials of the World Data Center B, Sovjet Geophysical Committee of the Academy of Sciences of the USSR, Moscow, 1986, 38 pp. (in Russian).
[32] T.H. Torsvik, D. Roberts, A. Siedlecka, Palaeomagnetic data from sedimentary rocks and dolerite dykes, Kildin Island, Rybachi, Sredni and Varanger Peninsulas, NW Russia and NE Norway: a review, Spec. Publ. - Nor. Geol. Unders. 7 (1995) 315–326.
[33] G. Bylund, Palaeomagnetism of the Late Precambrian Vadsø and Barents Sea Groups, Varanger Peninsula, Norway, Precambrian Res. 69 (1994) 81–93.
[34] V. Popov, A. Iosifidi, J. Tait, V. Bachtadse, A. Khramov, Neoproterozoic palaeogeography of Baltica: palaeomagnetic results from NW Russia, EGS XXVII General Assembly, Nize, France, abstract number EGS02-A-05990.
[35] K.M. Storetvedt, Remanent magnetization of some dolerite intrusions in the Egersund area, southern Norway, Geophys. Norv. 26 (1966) 17 pp.
[36] R.P.E. Poorter, Preliminary palaeomagnetic results from the Fen Carbonatite complex, S. Norway, Earth Planet. Sci. Lett. 17 (1972) 194–198.
[37] G. Vidal, M. Moczydlowska, The Neoproterozoic of Baltica — stratigraphy, palaeobiology and general geological evolution, Precambr. Res. 73 (1995) 197–216.